Journal of Power Sources 205 (2012) 86–92

Contents lists available at SciVerse ScienceDirect

Journal of Power Sources

journal homepage: www.elsevier.com/locate/jpowsour

Study of transformer-based power management system and its performance optimization for microbial fuel cells

Fan Yang[a], Daxing Zhang[b], Tsutomu Shimotori[c], Kuang-Ching Wang[a], Yong Huang[d,*]

[a] Department of Electrical and Computer Engineering, Clemson University, Clemson, SC 29634, USA
[b] School of Mechano-Electronic Engineering, Xidian University, Xi'an 710071, China
[c] Minnesota Department of Health, St. Paul, MN 55164, USA
[d] Department of Mechanical Engineering, Clemson University, Clemson, SC 29634-0921, USA

ARTICLE INFO

Article history:
Received 15 October 2011
Received in revised form
14 December 2011
Accepted 1 January 2012
Available online 20 January 2012

Keywords:
Microbial fuel cell
Optimization
Power management system
Super-capacitor
Wireless sensor

ABSTRACT

Microbial fuel cells (MFCs) are emerging as a promising alternative renewable energy source, especially for remote monitoring applications. Due to its low voltage and power output, MFCs are unable to directly drive most commercial electronic devices. A power management system (PMS) is needed to accumulate MFC energy first and then drive the load intermittently. In this study, a transformer-based PMS is proposed, which is able to function under a lower voltage input than other available MFC PMS designs. Two super-capacitors are included in the proposed PMS. The first is analytically optimized to maximize the average harvested power, while the second is selected based on the energy required to drive a given load. A continuous-mode MFC was built and used to successfully drive an IEEE 802.15.4 wireless sensor system using the proposed PMS. Experimental results showed that the proposed PMS worked well under a very low input voltage (0.18 V). The configuration of two super-capacitors and a transformer in this transformer-based PMS provides more flexibility in harvesting power from MFCs.

1. Introduction

Microbial fuel cells (MFCs) have been widely viewed as one of the sustainable energy harvesting apparatuses, and its basic principle is to use microorganisms as catalysts to convert chemical energy in the substrate into electrical energy [1]. An MFC is a bioelectrochemical system (BES) that generates electrical energy by the catalytic reaction of organic substrates such as wastewater using microorganisms [2,3]. MFCs, in either one or two chamber setups, generally consist of three parts: the anode, the cathode (usually separated by a membrane), and the electrolyte. A lower potential is induced at the anode through oxidation of its substrate using microorganisms, generating free electrons, while a higher potential is achieved at the cathode through a reduction process.

While MFCs are a promising renewable power source, hurdles remain for them to be widely adopted. Among them, their low power density and high internal resistance are two pronounced challenges in operation, resulting in a low output voltage and power. Typical MFCs may produce an open circuit voltage from 0.3 to nearly 0.9 V [4,5] mainly depending on the type of microorganisms and electrode materials. The power density of MFC usually ranges from 1 mW m^{-2} [6] to 2000 mW m^{-2} [7–9]. Unlike conventional power supplies such as batteries, which typically have a very low internal resistance (less than 1 Ω [10]), the internal resistance of MFC is relatively high (30–45 Ω [11–13] and 200–400 Ω [14]). Such a high internal resistance is due to activation loss, ohmic loss and concentration loss [3] and is quite a challenge to reduce it. As a result, a considerable portion of harvested energy is consumed internally instead of powering an external load [15,16]. It is challenging to directly power most electronic devices with MFCs.

Various attempts, such as serial stacking and DC/DC (direct current) boosting have been made to increase the MFC voltage. Serial stacking of MFCs has been proven to be difficult or ineffective [17] to implement in open water environments and may result in even lower voltage and power outputs due to the voltage reversal [18]. The simple idea of using a DC/DC converter to boost an MFC's output voltage is not applicable as the MFC output is too low to directly drive the DC/DC converter. Even if the DC/DC converter can work, there may be no sufficient energy left to drive the load directly [17]. Thus, a power management system (PMS) is usually required to interface an MFC with the load. The PMS for an MFC should be able to raise the voltage to a sufficient level and accumulate enough power to drive the load. Super-capacitors are commonly adopted to accumulate the MFC energy over a certain period and provide intermittent power to loads [17,19,20].

Current PMS designs for MFCs can be classified into two types: capacitor-converter type [19] and capacitor-charge pump-converter type [17,20]. The former type requires a high voltage

* Corresponding author. Tel.: +1 864 656 5643; fax: +1 864 656 4435.
E-mail address: yongh@clemson.edu (Y. Huang).

0378-7753/$ – see front matter © 2012 Elsevier B.V. All rights reserved.
doi:10.1016/j.jpowsour.2012.01.025

output from MFCs (usually more than 0.7 V), which is not easily achievable per most MFC outputs. The latter type lowers the input voltage requirement by increasing the super-capacitor voltage using a charge pump; however, a minimum input voltage such as 0.3 V (limited by typical charge pumps) is still needed for the charge pump to function.

This paper proposes a transformer-based PMS to further lower the input voltage requirement to around 0.2 V using two super-capacitors and a transformer. The rest of this paper is organized as follows. Section 2 reviews the background of MFC power management and capacitor optimization. The proposed transformer-based PMS and its optimization are introduced in Section 3. Section 4 presents experimental implementation and evaluation of the proposed PMS. The paper concludes in Section 5.

2. Background

PMS is widely used with various low-power energy harvesting systems, such as MFCs, small solar cells, or vibration and thermal energy generators, to adjust their output voltage or power. It is typically designed to boost a low-voltage input to a high-voltage output (e.g., 3.3 V) to continuously or intermittently drive commercial electronic devices. Most existing commercial DC/DC converters are designed to regulate much higher currents than a few mA that can be harvested from low-power energy sources such as MFCs. Generally, DC/DC converters are inefficient, if still operable, under such low currents.

Rechargeable batteries and super-capacitors are typical devices used in energy harvesting systems [17,19–21]. Compared with a super-capacitor, a rechargeable battery has a higher energy density but requires a significantly longer charging time [21]. A super-capacitor is more suitable for applications needing power intermittently for only fractions of a second to several minutes [22], which is the case of typical MFC-based electronic devices. The charging voltage for a super-capacitor can be continuously adapted to match the optimal rectifier voltage requirement of energy harvesting systems [23]. In addition, super-capacitors have a longer lifetime than that of rechargeable batteries [21,23]. As a result, super-capacitors have become more widely used in energy harvesting systems.

When capacitors are used as energy storage devices, the output power and charging/discharging cycle of a PMS are affected by the capacity of capacitors [24]. Determining the optimal capacitance of energy storage capacitors for MFC applications has been of great interest in order to maximize the usable MFC output power for a given duration. Once the PMS circuit is selected, the PMS performance is largely determined by the selection of associated super-capacitors. The optimization of super-capacitors has usually been conducted through effective, but laborious and time-consuming experimental investigations [24]. While some studies have yielded optimization methods for charging super-capacitors [25,26], most such methods require additional circuits or devices to manage the charging process, which is not feasible for MFCs due their low power output. Consequently, developing an effective and efficient optimization approach is critical for optimizing PMS performance, which is also a subject of this study.

3. Power management system design and performance optimization

This study aims to design a transformer-based PMS for low-voltage power sources such as MFCs. The study then proposes to optimize the PMS performance by selecting the appropriate capacitance for its super-capacitor such that the average power output for each charging/discharging cycle is maximized based on the equivalent circuit of MFC.

3.1. Proposed transformer-based power management system

Different PMSs for MFC power harvesting have been studied for intermittent load driving applications such as intermittent wireless transmission of sensed information. The simplest PMS can be implemented by directly connecting a super-capacitor to an MFC to increase and control the electrical potential generated by an MFC [19]; with this setup, however, the highest achievable output voltage is equal to the MFC output voltage, meaning that only very little energy can be stored and utilized per cycle. A simple improvement

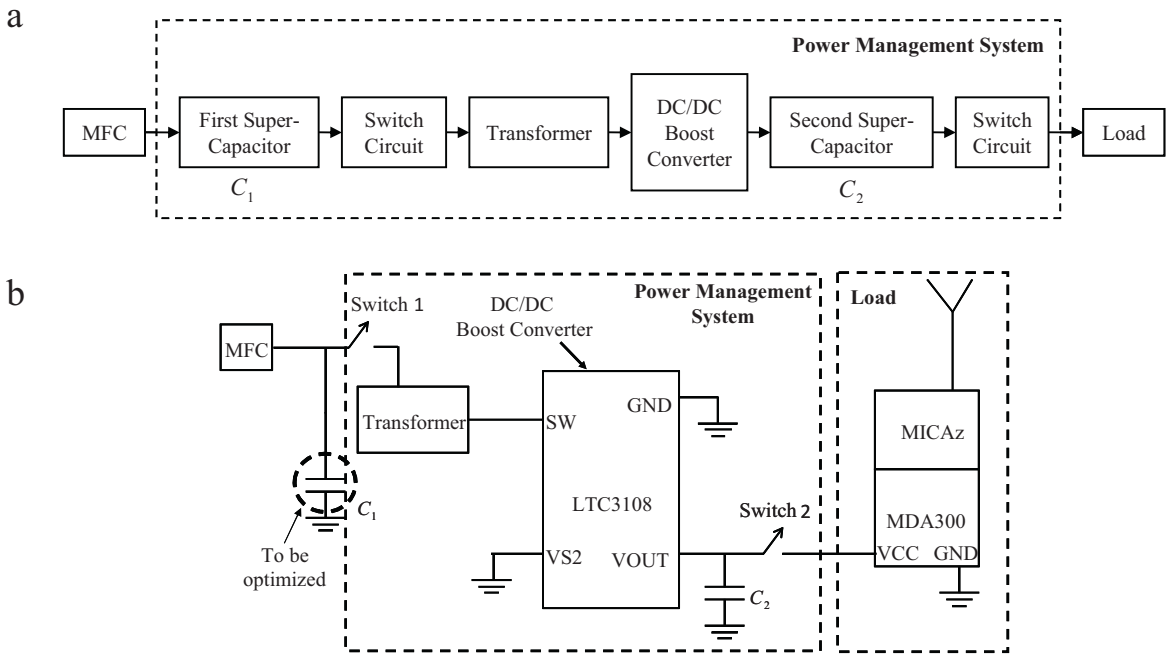

Fig. 1. (a) Transformer-based power management system and (b) PMS detailed circuit implementation.

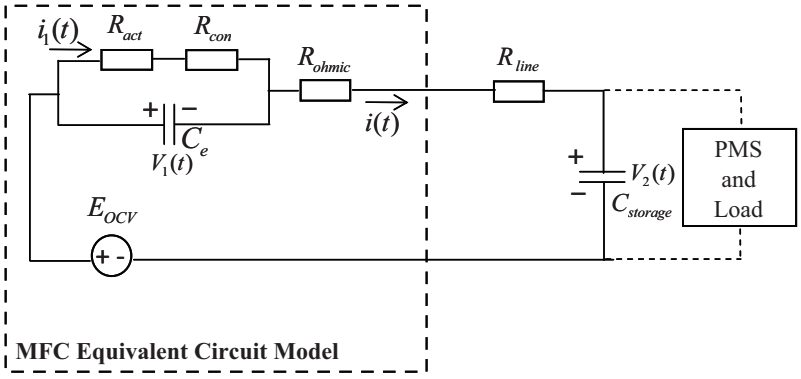

Fig. 2. Equivalent circuit model for MFC and the overall circuit schematic during charging.

can be made by adding a charge pump before the super-capacitor and a DC/DC converter after the super-capacitor, such that the load is driven only when a predefined threshold voltage is reached [17]. Such a PMS is good for MFCs' low-voltage outputs, but it only works if the MFC output voltage is high enough to drive the charge pump (e.g., 0.3 V). Its charging/discharging cycle is also much longer since the charging speed is limited by the charge pump.

To lower the input voltage requirement without sacrificing the charging speed, this study proposes to use a transformer to replace the charge pump as shown in Fig. 1. This capacitor-transformer-converter PMS circuit utilizes two super-capacitors: one is connected to the MFC, and the other is placed after the DC/DC converter. The first super-capacitor (C_1), which is to be optimized, accumulates energy from the MFC and drives the following DC/DC converter. The second super-capacitor (C_2), whose capacitance must be determined based on the target load, stores power from the DC/DC converter and drives the load in bursts with high voltage and current as demanded by different applications.

3.2. Capacitor optimization

In order to identify the optimal capacitance for the first super-capacitor, an MFC is modeled using an equivalent circuit as shown in Fig. 2. Numerous equivalent circuit models have been developed in prior studies to model the MFC behavior when an MFC is connected with an external load. The fuel cell internal resistance can usually be modeled as a combination of anodic resistance, cathodic resistance, and ohmic resistance [16], while the anodic and cathodic resistances may be current-dependent [27]. There is a capacitance at the interface between the electrode and its surrounding electrolyte/substrate when the charges in the electrode are separated from those in the electrolyte [28]. All these effects should be included to model an MFC electrically. Herein, an MFC is modeled as an ohmic resistor in series with a parallel combination of the electrode capacitor and the associated charge transfer resistors, which are related to the activation and concentration energy of the anode and cathode [29]. In Fig. 2, R_{act}, R_{con} and R_{ohmic} account for the equivalent resistance of the MFC activation loss, concentration loss, and ohmic loss, respectively, E_{OCV} is the MFC open circuit voltage, C_e represents the electrode capacitor, and R_{line} is the resistance of the peripheral circuitry.

As shown in Appendix A, the MFC polarization curve (voltage–current curve) can be described using an equivalent circuit:

$$V_{cell} = E_{OCV} - IR_{ohmic} - aT - bT\ \ln(I) + c\ln\left(1 - \frac{I}{I_{limit}}\right) \quad (1)$$

where I_{limit} is the MFC limiting current (also known as the maximum MFC current), T is the absolute temperature, and I is the current flowing through R_{ohmic}.

Since commercial DC/DC converters are commonly used to build a PMS, it is not convenient to modify the parameters of commercial converters for PMS performance optimization. Under such circumstances, only super-capacitors are considered reconfigurable for optimized average power generation. Using the equivalent circuit shown in Fig. 2, the following equations can be established based on the Kirchhoff and Ohmic laws:

$$\begin{cases} C_e\dfrac{dV_1(t)}{dt} = i(t) - i_1(t) \\ E_{OCV} - V_1(t) - i(t)R_{ohmic} = i(t)R_{line} + V_2(t) \\ C_{storage}\dfrac{dV_2(t)}{dt} = i(t) \\ i_1(t) = \dfrac{V_1(t)}{R_{act} + R_{con}} \end{cases} \quad (2)$$

where $V_1(t)$ is the voltage of the electrode capacitor, $V_2(t)$ is the voltage of the super-capacitor ($C_{storage}$, corresponding to C_1 of Fig. 1), $R_{act} = T[a + b\ln(i_1(t))]/i_1(t)$, $R_{con} = -c\ln(1 - (i_1(t)/I_{limit}))/i_1(t)$, and a, b, c, I_{limit} and R_{ohmic} are five unknown parameters to be experimentally determined. R_{act} and R_{con} can be estimated based on the MFC steady-state analysis. The initial values of $V_1(t)$ and $V_2(t)$ are both zero before the super-capacitor starts drawing energy from an MFC. When $V_2(t)$ reaches the discharging voltage V_d, the super-capacitor begins to discharge and drive the PMS and load until $V_2(t)$ drops to the charging voltage V_c for charging to begin again. During the steady state, the voltage on the super-capacitor $V_2(t)$ varies between V_d and V_c, and the average power stored in this voltage range is of interest in this study.

By solving Eq. (2), the charging time (T_c) for the super-capacitor to be charged from V_c to V_d can be obtained, with the average power input to the PMS and load being a function of $C_{storage}$:

$$P_a = \frac{1}{2T_c}C_{storage}(V_d^2 - V_c^2) \quad (3)$$

and the optimal capacitance is determined by maximizing P_a.

4. Experimental evaluation of proposed power management system

4.1. MFC experimental setup and characterization

4.1.1. MFC experimental setup

A single-chamber air-cathode MFC reactor was constructed as shown in Fig. 3, and the reactor had an anodic chamber volume of 316 ml. The anode was made of 0.381 mm thick carbon cloth (CCP30CM, Fuel Cell Earth, Stoneham, MA, USA). The cathode was made of 0.28 mm thick carbon paper (TGP-H-090, Fuel Cell Earth,

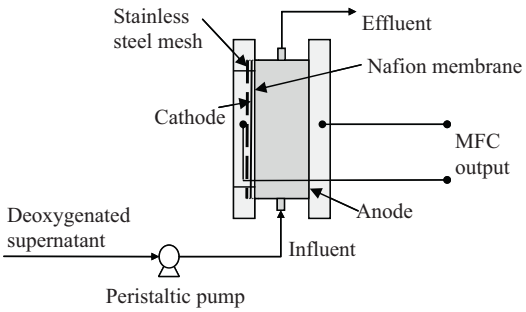

Fig. 3. Single-chamber air-cathode MFC reactor.

Stoneham, MA, USA), which was covered with Pt-catalyst (XC-72, Fuel Cell Store, Boulder, CO, USA). Each of the electrodes, apart by 2.5 cm and separated by a 0.18 mm thick Nafion membrane (N117, DuPont, Wilmington, DE, USA), had a diameter of 12.7 cm. The Nafion membrane was sequentially soaked in H_2O_2 (3%) at 50 °C, deionized water at 80 °C, 0.5 M H_2SO_4 at 50 °C, and deionized water at 80 °C (each for 1 h) immediately prior to the experiment. A piece of stainless steel mesh was used to prevent the deformation of the cathode.

Domestic wastewater bacteria have been shown to be suitable biocatalysts for MFC-based electricity production [30]. Anaerobic domestic wastewater (Greenville Wastewater Treatment Plant, Greenville, SC, USA) was used as both the inoculum and the substrate during the inoculation process. Additional nutrient medium was prepared to mix with the anaerobic wastewater at the ratio of 1.5:1. The deionized water-based medium, around PH 7, was prepared as follows (per liter): 310 mg NH_4Cl, 130 mg KCl, 2690 mg $NaH_2PO_4{\cdot}H_2O$, 4330 mg Na_2HPO_4, 1510 mg NaCl, 0.15 mg $FeCl_2{\cdot}4H_2O$, 0.006 mg H_3BO_3, 0.009 mg $MnSO_4{\cdot}H_2O$, 0.012 mg $Co(NO_3)_2{\cdot}6H_2O$, 0.0132 mg $ZnSO_4{\cdot}7H_2O$, 0.0025 mg $NiCl_2{\cdot}6H_2O$, 0.0014 mg $CuCl_2$, 0.0025 mg $Na_2MoO_4{\cdot}2H_2O$, 0.00088 ml 37% HCl and 4 ml sodium acetate (Sigma–Aldrich, St. Louis, MO, USA).

During inoculation, the MFC reactor was first filled with the anaerobic domestic wastewater and nutrient medium solution and was operated under the batch mode. With an external 1 kΩ resistor connected, the MFC output voltage increased from zero and surpassed 0.605 V, and a rapid current increase was observed. The inoculation process was considered finished after the output voltage had stayed around 0.605 V for five days.

After inoculation, the inoculation solution was replaced with deoxygenated wastewater supernatant (Clemson Wastewater Treatment Plant, Clemson, SC, USA), 10 mM sodium acetate, and 30 mM NaCl. Acetate was added to avoid the substrate limitation on current in that the study of such limitations is beyond the scope of this study. The resulting supernatant-based substrate was approximately pH 6.4. This substrate was continuously instilled into the MFC reactor using a peristaltic pump (Cole-Parmer, Chicago, IL, USA) at 0.4 ml min^{-1} (equivalent a hydraulic retention time (HRT) of 13.2 h in this study). The entire experiment was performed with a 1 kΩ resistor connected under room temperature.

4.1.2. Identification of MFC equivalent circuit and optimal capacitance

Once the MFC reactor reached the steady state after three days under a continuous mode, the 1 kΩ resistor was disconnected to measure the MFC open circuit voltage (OCV), which was around 0.79 V in this study. Then a series of resistors were connected to the MFC reactor with the resistance progressively changed from 10 kΩ to 50 Ω every 10 min to obtain the MFC polarization curve. Ten minutes were sufficient for the MFC reactor to reach the steady state after each resistance change in this study. The resulting voltage was continuously recorded using a multimeter (34410A, Agilent,

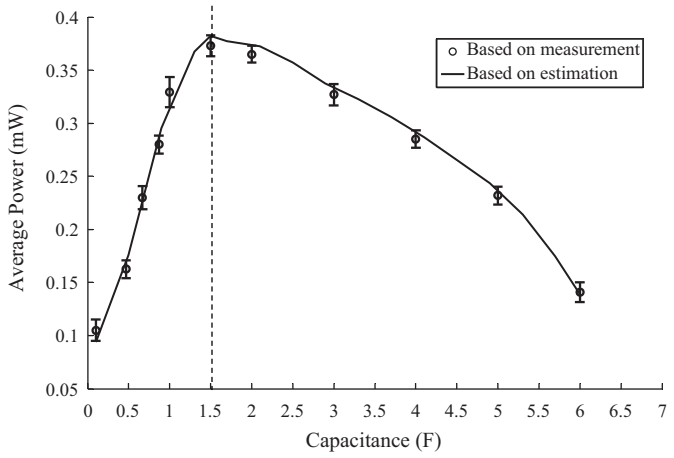

Fig. 4. Measured and estimated average stored power at different capacitance values.

Santa Clara, CA, USA) during this process, and the associated current was calculated by dividing the recorded voltage by the external resistance.

For the MFC polarization curve, represented by Eq. (1), E_{OCV} was measured once the MFC reactor was functional, the absolute temperature was 297 K, and the five unknown parameters were estimated by curve fitting based on Eq. (1). The parameter estimates are: $R_{ohmic} = 221.52\ \Omega$, $I_{limit} = 0.002$ A, $a = 3.6e^{-4}$, $b = 2.7e^{-5}$, and $c = 0.3568$. The identified R_{ohmic} is close to that of a similar MFC study [31], which was found to be 218 Ω. The value of C_e can be found by fitting the equivalent model to the Nyquist plot of the dynamic impedance measurement [32] or the MFC voltage response during the transient period after the step-down change of current [33] in addition to the cyclic voltammetry [3]. For convenience, the capacitance of the electrode capacitor C_e was estimated using the transient voltage response method proposed in [33]. During the estimation process, a 5 kΩ external resistor was first connected to the MFC until the steady state was reached. The voltage was recorded as the initial voltage, and the 5 kΩ resistor was replaced with a 10 kΩ resistor. The voltage of the external resistor increased (compared with the initial voltage) and finally reached the steady state about 20 min later. The resulting transient voltage responses were recorded accordingly, and the voltage difference curve was fitted with the function proposed in [33]. The identified capacitance (C_e) is 0.0042*F*. It should be noted that the curve fitting method is not a reliable method to accurately identify each single unknown parameter while it does work in identifying MFC parameters [33,34]. For accurate determination of electrochemical parameters, traditional electrochemical techniques, such as the current interrupt test and the cyclic voltammetry [3], should be adopted.

The optimal capacitance of the first super-capacitor was found as 1.5 F by maximizing P_a based on the equivalent MFC parameters and Eq. (3). Further experiments were conducted to validate this estimated optimal capacitance. The capacitance of the first super-capacitor was changed from 0.1 F to 6 F (at 0.1, 0.47, 0.67, 0.87, 1, 1.5, 2, 3, 4, 5 and 6 F). At each value, the capacitor was connected to the MFC directly, and then the charging process began. In the steady state, when the voltage of the capacitor (V_2) was raised from the charging voltage (V_c) to the discharging voltage (V_d), the charging time T_c was recorded. The average power P_a harvested during a single charging cycle was then calculated based on Eq. (3). The same procedure was repeated three times for each capacitance. The experimental results are shown in Fig. 4, and the optimal capacitance is the one that results in the maximum average power. From Fig. 4, the power estimation curve matches the measurement

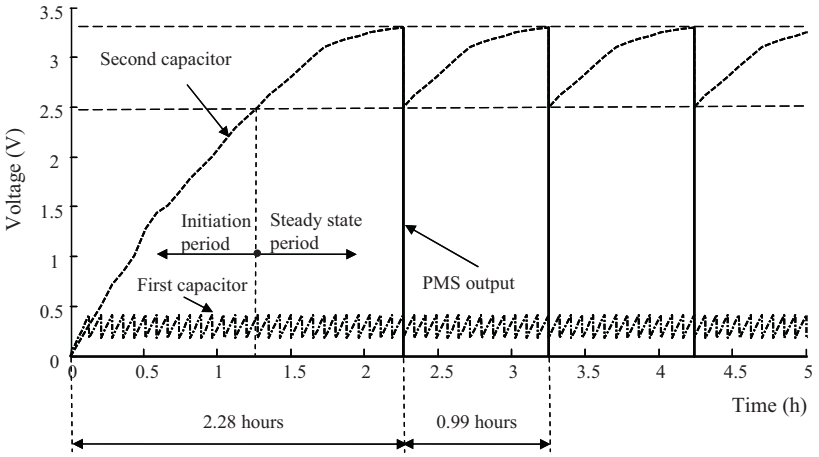

Fig. 5. Voltage on the capacitors and output of PMS.

results very well, demonstrating the effectiveness of the proposed optimization methodology. Both the analytical and experimental studies have found that the 1.5 F super-capacitor works the best for maximum average power harvesting for the MFC reactor in this study. As seen, the proposed optimization method is a simple and effective approach for finding the optimal capacitance instead of the time-consuming experimental approach.

4.2. PMS circuit implementation

The detailed design of the proposed PMS circuit is shown in Fig. 1(b). The voltage step-up converter used was LTC3108 (Linear Technology, Milpitas, CA, USA) [35]. The first super-capacitor (C_1) is first charged by the low-voltage output of the MFC, and Switch 1 is utilized to prevent the transformer and LTC3108 from drawing current from the first super-capacitor while it is being charged. Switch 1 is comprised of a Germanium transistor and an ALD110800 MOSFET (Advanced Linear Device, Sunnyvale, CA). The selected MOSFET has a typical zero gate threshold voltage.

The discharging voltage V_d is the rising threshold voltage of the Germanium transistor, and the charging voltage V_c is the falling threshold voltage of the transistor. When the voltage of the super-capacitor reaches the turn-on voltage of the switch (0.41 V, discharging voltage V_d), the transistor functions and a voltage difference is applied at MOSFET, which makes MOSFET work and Switch 1 close. After Switch 1 closes, the first super-capacitor works as the energy source to power the rest of the PMS system and load. The voltage of the first super-capacitor is then amplified by the transformer (LPR6235-752SML, Coilcraft, Cary, IL, USA). The amplified voltage is then rectified by an internal rectifier circuit. While the first super-capacitor discharges, the second super-capacitor (C_2) then begins the charging cycle.

Switch 1 remains closed until the input voltage drops to V_c (0.18 V), which makes the transistor completely shut. Once Switch 1 is open, the first super-capacitor begins being charged again. This process iterates until the voltage of the second super-capacitor reaches a target voltage specified by the application (such as 3.3 V for a typical wireless sensor device). Then Switch 2 closes to power the application load. Switch 2 is used to prevent the load from drawing current from the second super-capacitor before it reaches the target voltage.

To demonstrate the feasibility of the proposed transformer-based PMS, the energy harvested from the MFC was used to power the MDA300 sensor board and the MICAz wireless sensor node (Moog Crossbow, Milpitas, CA, USA) [36,37] using the PMS as shown in Fig. 1(b). Embedded with temperature and humidity sensors, MDA300 can measure environmental data such as temperature and humidity. MICAz is used for wireless transmission of the data collected by MDA300. The total power consumption is approximately 65 mW for MICAz transmission at 0 dBm transmit power and 30 mW for MDA300 sensing. The proposed PMS stores the MFC harvested energy to achieve an intermittent 3.3 V output sufficient for driving the wireless sensor node. To support transmission of three 90-bytes packets in each charging cycle, the second super-capacitor was selected as 0.05 F. It should be noted that the capacitance of the second super-capacitor is dependent on the power need of loads. An LTC3108 converter with a peripheral circuit as described in the LTC3108 datasheet [35] was utilized in the test setup.

4.3. Experimental evaluation of transformer-based PMS

During PMS operation, the 1.5 F (optimal value) super-capacitor C_1 was charged to 0.41 V and discharged to about 0.18 V. The measured average charging time was about 273 s (±5). This charging time is comparable to that of other similar studies. For example, Shantaram et al. [19] charged a 4 F capacitor from 0 to 0.5 V in 2 min using an MFC with a 265 cm^2 surface area sacrificial anode. Since a smaller surface area (127 cm^2) MFC was used in this study, a longer charging time was expected. Moreover, in [20], a 10 F capacitor needed approximately 10 min to charge from 0 to 0.5 V using a sediment MFC with a 0.2 m^2 projected surface area.

During the experiment, the charging and discharging voltage history was studied based on the wireless sensing setup. When the first super-capacitor was charged to the discharging voltage, Switch 1 closed and the PMS began to charge the second super-capacitor. After the voltage of the first super-capacitor dropped to the charging voltage, it was charged by the MFC again. This charging and discharging process was repeated until the second 0.05 F capacitor was charged from 0 V to 3.3 V, which was equivalent to about 2.28 h. After that Switch 2 closed and the power accumulated in the second super-capacitor was discharged to drive the load. This discharging process continued until the voltage on the second capacitor dropped below 2.5 V, under which the load (MICAz with MDA300) was no longer working. The minimum input voltage for MICAz with MDA300 sensor board shown in [37] is 2.7 V, however, 2.5 V was the minimal input voltage value that was measured during the experimental tests herein. After the load was no longer working, the second super-capacitor was again charged until its voltage reached 3.3 V. Fig. 5 shows the voltages on the

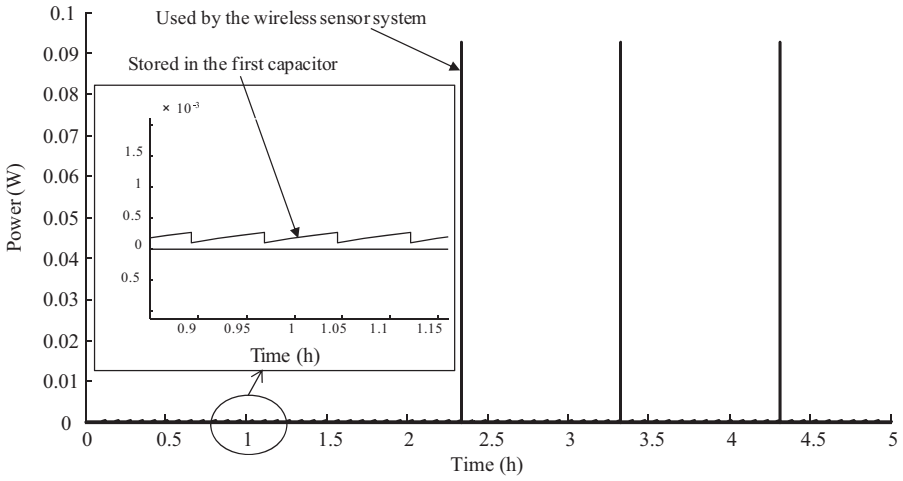

Fig. 6. Power stored in the first capacitor and delivered to the load.

capacitors and output of the PMS in the first three cycles. It took about 0.99 h to charge the second capacitor from 2.5 V to 3.3 V and this charging period is called the steady state period, which is repeated as charging/discharging cycles. As the initial voltage on the second super-capacitor is 0 V, the period when its voltage increases from 0 V to 2.5 V is referred as the initiation period.

In addition, the energies stored in the capacitors and delivered in the first three cycles were also measured and shown in Fig. 6 based on the power information. The first super-capacitor drew less than 0.4 mW from the MFC while the wireless transmitter and sensor board drew up to 95 mW power from the PMS when Switch 2 was closed.

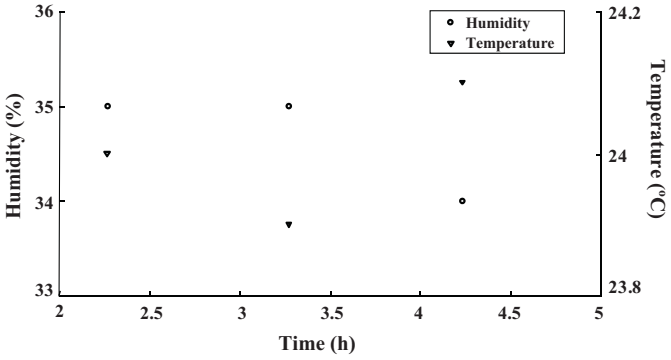

Fig. 7. Wireless sensor measurement results.

4.4. Wireless sensing application

Wireless transmission of temperature and humidity information using the PMS-assisted MFC was studied as an experimental application. As aforementioned, MICAz and MDA300 were attached together so that the temperature and humidity data sampled by MDA300s internal sensors can be included in MICAz's transmitted packets. When the voltage of the second capacitor reached 3.3 V and thus Switch 2 closed, MICAz was able to start up and transmit three packets. The reason to only transmit three packets is that for typical wireless sensor network applications, at least 2 packets are required for notification and handshake between neighbor sensors and one packet is needed to transmit information data. As shown in Fig. 6, it took about more than 2 h for the second super-capacitor to reach 3.3 V if its initial voltage was 0 V. However, the time interval during the steady-state charging/discharging cycles was about 0.99 h as the voltage of the second super-capacitor decreased to 2.5 V instead of 0 V, which greatly shortened the charging time of the second super-capacitor. Three representative cycles of wireless humidity and temperature measurements at the Clemson Advanced Manufacturing & Systems Integration Laboratory (Clemson, SC, USA) are shown in Fig. 7. One humidity data and one temperature data were transmitted in a single charging/discharging cycle. The time interval between charging/discharging cycles was measured as 0.99 h.

Similar wireless data transmission has also been tested in [20]. The wireless transmitter chosen was a Madgetech wireless temperature sensor (RFTC4000A, MadgeTech, Warner, NH, USA). Its RF carrier frequency is 418 MHz and its output power consumption is less than 1 mW. There were seven cycles of data transmission in 160 min, which indicates a shorter charging/discharging cycle than the proposed PMS in this study. However, as the load in this work consumed more than 90 mW power, 0.99 h charging/discharging cycle was already comparable. Moreover, in [17], a hydrophone with similar power consumption (95 mW) was used as the load and its charging/discharging cycle was around 9.3 h, indicating a great charging/discharging cycle performance of the proposed power management system.

The second super-capacitor of 50 mF was picked to provide sufficient energy to transmit three packets in this study. It should be noted that this capacity can be varied according to load requirements. Generally speaking, a larger capacity of the second super-capacitor results in a larger number of packets which

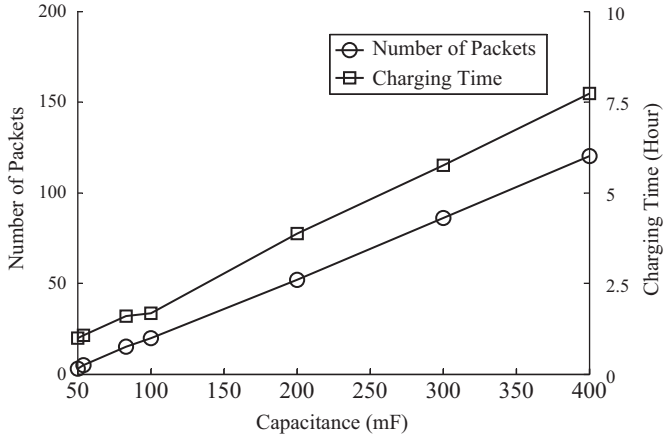

Fig. 8. Capacitance vs. number of packets and charging time.

can be transmitted during a charging/discharging cycle. Of course, the charging time also increases accordingly. The second super-capacitor was varied in terms of its capacity (50, 54.2, 83.3, 100, 200, 300, and 400 mF) to test the number of packets transmitted and the charging time during the steady state period. The experimental measurements are shown in Fig. 8, and it can be seen that both the number of packets transmitted and the charging time increase linearly with the capacity of the second super-capacitor. It means that once a load is identified, the second super-capacitor can be selected based on the energy need of the load.

5. Conclusions

While the power generating capacity of MFCs can be improved in terms of using different membrane/electrode materials and/or choosing different electrode sizes, a PMS is always essential to enhance the energy harvesting and usage efficiency. In this study, a transformer-based PMS is proposed to function under a lower voltage input than other available MFC PMS designs. Two super-capacitors are included in the proposed PMS. The first super-capacitor can be analytically optimized to maximize the average harvested power, and the second super-capacitor can be selected based on the energy required to drive a load. It is concluded that the proposed PMS works well under a very low input voltage (0.18 V) and can successfully drive an IEEE 802.15.4 wireless sensor device. The working duration of the powered sensing system is proportional to the capacity of the second super-capacitor. With two super-capacitors and a transformer in the proposed system, the proposed transformer-based PMS provides more flexibility in harvesting power from MFCs.

It should be noted that the applicability of super-capacitors may be dependent on the purpose and type of the MFC system, where the self-discharge rate does not impact the performance of the MFC application. Future work may include the accurate identification of each electrochemical parameter using electrochemical techniques rather than curving fitting, the comparison of the proposed transformer-based PMS with other counterparts, especially in terms of the energy efficiency, and the development of wireless sensor network protocols when using the proposed PMS.

Acknowledgements

The authors would like to thank Changxue Xu, Wenxuan Chai, and Jianing Dai of Clemson University for their experimental support, Dr. David Freedman of Clemson University for technical advice, and Angela Allen of the Greenville Wastewater Treatment Plant for wasterwater use. D. Zhang acknowledges the support of the Fundamental Research Funds for the Central Universities (K50511040010).

Appendix A. MFC polarization curve

Under practical operating conditions, the MFC output voltage V_{cell} is less than its open circuit voltage (E_{OCV}), mainly due to the activation loss, ohmic loss and concentration loss [29]:

$$V_{cell} = E_{OCV} - V_{act} - V_{ohmic} - V_{con} \quad \text{(A1)}$$

where V_{act}, V_{ohmic}, and V_{con} represent the activation, ohmic and concentration voltage drops, respectively, and are functions of the MFC current as seen from the MFC polarization curve, which is also known as the voltage–current curve (U–I curve). The activation loss is usually estimated using the Tafel equation [28]:

$$V_{act} = T[a + b\ln(I)] \quad \text{(A2)}$$

where T is the absolute temperature, a and b are the coefficients to be identified, and I is the current. Since the estimation of R_{con}, R_{act} and R_{ohmic} is based on the steady-state analysis, there is no current flowing through the electrode capacitor C_e. As such, the current flowing through these resistors is identical, and the Ohmic loss can be estimated as follows:

$$V_{ohmic} = IR_{ohmic} \quad \text{(A3)}$$

and the concentration loss can be represented [28]:

$$V_{con} = -\frac{RT}{nF}\ln\left(1 - \frac{I}{I_{limit}}\right) \quad \text{(A4)}$$

where R is the universal gas constant, n is the number of electrons per reaction mol, F is the Faraday constant, and I_{limit} is the limiting current of an MFC. Then the polarization curve can be simplified as follows:

$$V_{cell} = E_{OCV} - IR_{ohmic} - aT - bT\ \ln(I) + c\ln\left(1 - \frac{I}{I_{\lim it}}\right) \quad \text{(A5)}$$

References

[1] K. Rabaey, L. Angenent, Bioelectrochemical Systems: From Extracecellular Electron Transfer to Biotechnological Application, IWA Publishing, 2010.
[2] R.M. Allen, H.P. Bennetto, Appl. Biochem. Biotechnol. 39–40 (1993) 27–40.
[3] B.E. Logan, B. Hamelers, R. Rozendal, U. Schroder, J. Keller, S. Freguia, P. Aelterman, W. Verstraete, K. Rabaey, Environ. Sci. Technol. 40 (2006) 5181–5192.
[4] Z.W. Du, H.R. Li, T.Y. Gu, Biotechnol. Adv. 25 (2007) 464–482.
[5] B.E. Logan, Microbial Fuel Cells, 1st ed., Wiley-Interscience, John Wiley & Sons, Inc., 2008.
[6] A.K. Manohar, F. Mansfeld, Electrochim. Acta 54 (2009) 1664–1670.
[7] H. Liu, S. Cheng, B.E. Logan, Environ. Sci. Technol. 39 (2005) 658–662.
[8] E. Simon, C.M. Halliwell, C.S. Toh, A.E.G. Cass, P.N. Bartlett, J. Electroanal. Chem. 538–539 (2002) 253–259.
[9] S. Cheng, H. Liu, B.E. Logan, Environ. Sci. Technol. 40 (2006) 2426–2432.
[10] S. Sato, A. Kawamura, Proc. Power 2 (2002) 565–570.
[11] X.X. Cao, P. Liang, X. Huang, Acta Sci. Circumstantiae 26 (2006) 1252–1257.
[12] B. Min, I. Angelidaki, J. Power Sources 180 (2008) 641–647.
[13] P.Y. Zhang, Z.L. Liu, J. Power Sources 195 (24) (2010) 8013–8018.
[14] Y. Fan, E. Sharbrough, H. Liu, Environ. Sci. Technol. 42 (2008) 8101–8107.
[15] N. Nwogu, Basic Biotechnol. J. 3 (1) (2007) 73–79.
[16] P. Liang, X. Huang, M.Z. Fan, X.X. Cao, C. Wang, Appl. Microbiol. Biotechnol. 77 (2007) 551–558.
[17] A. Meehan, H.W. Gao, Z. Lewandowski, IEEE Trans. Power Electron. 6 (1) (2011) 176–181.
[18] S.E. Oh, B.E. Logan, J. Power Sources 167 (2007) 11–17.
[19] A. Shantaram, H. Beyenal, R. Raajan, A. Veluchamy, Z. Lewandowski, Environ. Sci. Technol. 39 (2005) 5037–5042.
[20] C. Donovan, A. Dewan, D. Heo, H. Beyenal, Environ. Sci. Technol. 42 (2008) 8591–8596.
[21] M.J. Guan, W.H. Liao, J. Intell. Mater. Syst. Struct. 19 (2008) 671–680.
[22] R.J.M. Vullers, R.V. Schaijk, I. Doms, C.V. Hoof, R. Mertens, Solid State Electron. 53 (2009) 684–693.
[23] I. Buchmann, Batteries in a Portable World: A Handbook on Rechargeable Batteries for Non-Engineers, 2nd ed., Cadex Electronics Inc., Richmond, Canada, 2001.
[24] A. Dewan, C. Donovan, D. Heo, H. Beyenal, J. Power Sources 195 (2010) 90–96.
[25] J.C. Chen, Int. J. Electron. 88 (2001) 145–151.
[26] M.M. Peretz, S.B. Yaakov, Energy Convers. Congr. Exposition (2009) 1118–1125.
[27] M. Ceraolo, C. Miulli, A. Pozio, J. Power Sources 113 (1) (2003) 131–144.
[28] J. Larminie, A. Dicks, Fuel Cell Systems Explained, 2nd ed., John Wiley & Sons Ltd, 2003.
[29] C. Wang, M.H. Nehrir, S.R. Shaw, IEEE Trans. Energy Conversion 20 (2) (2005) 442–451.
[30] D.H. Park, J.G. Zeikus, Biotechnol. Bioeng. 81 (3) (2003) 348–355.
[31] H. Liu, B.E. Logan, Environ. Sci. Technol. 38 (2004) 4040–4046.
[32] E. Laffly, M.C. Pera, D. Hissel, Conf. Rec. IEEE Int. Symp. Ind. Electron, 2008, pp. 1519–1524.
[33] P.T. Ha, H. Moon, B.H. Kim, H.Y. Ng, I.S. Chang, Biosens. Bioelectron. 25 (2010) 1629–1634.
[34] M.T. Outeiro, R. Chibante, A.S. Carvalho, A.T. de Almeida, J. Power Sources 185 (2008) 952–960.
[35] Ultralow Voltage Step-Up Converter and Power Manager, Linear Tech. Corp., 2010.
[36] MDA300, Crossbow Technology Inc., Available online at: http://www.cens.ucla.edu/~mhr/daq/datasheet.pdf (accessed on 30th September 2011).
[37] MICAz Wireless Measurement System, Crossbow Technology, Inc. Available online at: http://www.openautomation.net/uploadsproductos/micaz_datasheet.pdf (accessed on 30th September 2011).